Available online at www.sciencedirect.com
ScienceDirect
Trans. Nonferrous Met. Soc. China 29(2019) 1763−1775
Transactions of Nonferrous Metals Society of China
www.tnmsc.cn

Selenium(VI) removal from caustic solution by synthetic Ca−Al−Cl layered double hydroxides

Shao-dong XU, Dong LI, Xue-yi GUO, Wen YAN, Jie GAO

School of Metallurgy and Environment, Central South University, Changsha 410083, China

Received 1 December 2018; accepted 10 June 2019

Abstract: To extract selenium(VI) from the highly caustic leachate of copper anode slime, the Ca−Al−Cl layered double hydroxides (Ca−Al−Cl−LDHs) with a formula of $Ca_2Al(OH)_6Cl{\cdot}2H_2O$ by three co-precipitation methods were synthesized. A plate-like morphology and hexagonal crystal structure with typical mineral phases and functional groups were identified by the FESEM, XRD, FTIR, BET and XPS analysis. The forward feeding sample exhibits the best adsorption capacity of Se(VI). The factor experiments then reveal a favorable adsorption process with low temperature, low NaOH concentration and high adsorbent dosage. Furthermore, the adsorption kinetics and isotherm parameters can be well described by the Langmuir isotherm and the pseudo-second-order models, respectively. Accordingly, the maximum adsorption amount of Se(VI) onto Ca−Al−Cl−LDHs reaches 188.6 mg/g at 50 °C.

Key words: copper anode slime; layered double hydroxide; selenium adsorption; kinetics; isotherm

1 Introduction

In metallurgy industry, the natural resource of selenium and selenium compounds is scarce. Typically, selenium can be present in the copper anode slime with a high richness ranging in 8%−20% [1,2]. With the increasing demands to extract selenium, several strategies have been developed including sulfidation roasting, oxidation roasting and soda roasting method [1,3]. However, these extraction methods not only exhibit a low extraction efficiency, but also generate several contaminants such as SO_2 [4]. Therefore, alkaline pressure leaching of copper anode slime gains emerging interests due to its high extraction efficiency and complete separation of selenium from concomitant metals [3]. It is noted that a large number of highly caustic solutions are also generated in this process, the extraction of selenium(VI) before further recycling of alkali is solely needed [5].

The extraction methods have been widely investigated in the past decades, including ion exchange, coagulation or coprecipitation, and adsorption process [6−8]. Typical coprecipitation method is limited by the harsh operation condition and restrict initial selenium(VI) concentration. Therefore, the adsorption strategy including a sequential process of adsorption, desorption and reduction to produce metallic selenium becomes popular [3,9]. It is noted that common adsorbent materials including iron hydroxides, molecular sieve and active carbons all exhibit a relatively low deselenization efficiency and low cost-effectiveness [10,11], layered double hydroxides (LDHs), known as the anion-exchange clay materials, have attracted wide interests due to their high efficiency and operability [3]. LDHs are usually composed of positively charged brucite-like sheets and negatively charged anions in the hydrated interlayer regions with the formula of $[A^{II}_{1-x}B^{III}_x(OH)_2]^x(A^{n-})_{x/n}\cdot mH_2O$. A^{II} usually represents Ca^{2+}, Mg^{2+}, Zn^{2+}, Cu^{2+}, etc. B^{III} is trivalent cations such as Al^{3+}, Fe^{3+} and Cr^{3+}. A^{n-} then denotes the exchangeable interlayer anion of Cl^-, NO_3^-, CO_3^{2-}, etc, while m is the number of interlayer water [12]. Due to the weak interlayer bonding, LDHs can adsorb anions through both surface adsorption and anion exchange [13,14]. Among diverse LDHs, a familiar group of Friedel's salts (also known as Ca−Al−Cl−LDHs) are the promising candidates with the trigonal crystals of a flat hexagonal structure [3,15]. Owning to the ion exchange characteristic of Cl^- with

Foundation item: Project (51604303) supported by the National Natural Science Foundation of China
Corresponding author: Dong LI; Tel: +86-731-88876255; E-mail: dongli@csu.edu.cn
DOI: 10.1016/S1003-6326(19)65084-3

other anions, Ca−Al−Cl−LDHs have been widely studied in recent years, exhibiting the adsorption behaviors on AsO_4^{3-} and CrO_4^{2-} [16,17]. Also, Ca−Al−Cl−LDHs can act as a cost-efficient absorbent for selenium removal in the acidic liquid, reaching a deselenization efficiency of 90% [18]. However, to our knowledge, the adsorption behavior of Se(VI) onto Ca−Al−Cl−LDHs in the highly caustic solution with high selenium content has not been investigated, although this is important for the practical extraction of selenium from copper anode slime leachate.

Herein, the effort to apply Ca−Al−Cl−LDHs on the adsorption of Se(VI) in the alkaline condition was made. Specifically, Ca−Al−Cl−LDHs were synthesized by a co-precipitation method with three different adding sequences, and their optimum feeding mode was determined through the preliminary adsorption experiment. Factor experiments including the adsorption temperature, adsorbent material dosage and NaOH concentration were also studied. A series of characterizations of Ca−Al−Cl−LDHs collected before and after adsorption were further performed. Se(VI) adsorption kinetics and isotherms were investigated and different adsorption models were used to evaluate the experimental data.

2 Experimental

2.1 Materials

All reagents were of analytical grade (Sinopharm Chemical Reagent Co., Ltd., Shanghai, China). Especially, the Se(VI) stock solution was prepared from the sodium selenate (Na_2SeO_4) with distilled water.

2.2 Preparation of Ca−Al−Cl−LDHs

The Ca−Al−Cl−LDHs were prepared by a coprecipitation method. Typically, the precipitation experiment was conducted in a 1 L round-bottomed flask with four necks, a two-blade mixer and thermostat water bath. The preparation experiments were conducted by preheating 300 mL mixed solution containing 0.5 mol/L $CaCl_2$ and 0.25 mol/L $AlCl_3$ to 50 °C. The equal volume of 1.5 mol/L NaOH was also added at a rate of 2 mL/min with a peristaltic pump and whilst stirring at 300 r/min. When the adding process was completed, the stirring continued for 1 h. Particularly, three feeding methods including forward feeding (FF), backward feeding (BF) and parallel feeding (PF) methods to decide the adding sequence of the NaOH solution and mixed solution, were performed. The FF method meant adding the NaOH solution to the mixed solution, whereas the BF method required the adverse adding sequence. These two solutions were simultaneously added in the PF method. The resultant precipitate was then collected, washed with ultrapure water and dried at 50 °C overnight.

2.3 Characterization

The Se(VI) concentration was determined by Optima 2100DV Inductively Coupled Plasma Optical Emission Spectrometry (ICP−OES). The morphological and structural characterizations of Ca−Al−Cl−LDHs collected before and after adsorption were performed with X-ray diffraction (XRD, TTR III X-ray diffractometer), scanning electron microscope (SEM, JSM−6360LV spectrometer). Fourier transform infrared (FT-IR) spectroscopy was further obtained with a Nicolet 380 spectrometer (Thermo, USA). Surface element analysis was studied by X-ray photoelectron spectroscopy (XPS, Thermo 250X). The N_2 adsorption−desorption isotherms were measured by the Autosorb iQ Station (Quantachrome) and the specific surface area was calculated according to the Brunauer−Emmett−Teller (BET) model.

2.4 Adsorption experiments and analytical methods

The adsorption experiment of Se(VI) was conducted in the abovementioned flask reactor. The typical alkaline selenium solution contained 2 g/L Se(VI) and 40 g/L NaOH. The adsorption capacities of LDHs yielded from three feeding modes were firstly evaluated. Typically, 20 g absorbent samples were mixed with 500 mL alkaline selenium solution and the adsorption system was kept at 50 °C and 300 r/min. 5 mL samples were taken at 0, 30 and 120 min and immediately filtrated (0.45 μm). The filtrate was then acidized to pH=1.0 and diluted to 50 times before the ICP detection. The factor experiments were conducted as follows: (1) For the impacts of adsorption temperature, the adsorption temperatures were specially set to 30, 50, 70, 80 and 90 °C, respectively; (2) For the impacts of NaOH concentration, the NaOH concentrations in the selenium solution were specially set to 40, 60, 80 and 100 g/L, respectively; (3) For the impacts of the adsorbent dosages, the adsorbent dosages were set to 10, 20, 30 and 40 g/L.

The adsorption capacity (Q, mg/g) and deselenization efficiency (Y, 100%) were assessed by the following equations [19]:

$$Q=\frac{(C_0-C_e)V}{m} \tag{1}$$

$$Y=\frac{(C_0-C_e)}{C_0}\times 100\% \tag{2}$$

where V is the volume of Se(VI) solutions (L), m is the mass of adsorbent (g), C_0 and C_e represent the initial and equilibrium concentrations (g/L) of Se(VI), respectively. The adsorption kinetics and isotherms were conducted to evaluate the adsorption capacity of Se(VI) on LDHs. The first and pseudo-second order kinetic models were

employed to test the kinetic process of adsorption, while the mathematical expressions were depicted in Eqs. (3) and (4), respectively [20]:

$$\ln (q_e-q_t)=\ln q_e+k_1t \quad (3)$$

$$\frac{t}{q_t}=\frac{1}{k_2q_e^2}+\frac{t}{q_e} \quad (4)$$

where k_1 and k_2 are the first and second order adsorption rate constants, respectively; the q_e and q_t (mg/g) are the amounts of Se(VI) adsorbed per unit mass of adsorbent at equilibrium and time t, respectively. Langmuir (Eq. (5)) and Freundlich (Eq. (6)) isotherm equations were used to test the isotherm process of adsorption as follows [21]:

$$q_e=q_m\frac{K_LC_e}{1+K_LC_e} \quad (5)$$

$$q_e=K_FC_en_F \quad (6)$$

where for the Langmuir isotherm model, q_m is the maximum adsorption capacity of Se(VI) on Ca−Al−Cl−LDHs, C_e is the equilibrium concentration of Se (VI) in the liquor and K_L is the Langmuir constant, which can be calculated from the slope and intercept of plots of C_e/q_e versus C_e. For the Freundlich isotherm model, K_F represents the adsorption capacity of Se(VI) when the equilibrium concentration of Se(VI) equals 1 and n_F represents the dependence degree of adsorption with the equilibrium concentration of Se (VI), which can be obtained by a plot of ln q_e against ln C_e.

3 Results and discussion

3.1 Characterization of as-prepared LDHs via three feeding methods

To evaluate the impacts of different feeding methods, the as-prepared LDHs via forward feeding (FF), backward feeding (BF) and parallel feeding (PF) methods were characterized by a combined FESEM, BET, XRD, FT-IR, and XPS analysis. FESEM images in Fig. 1 exhibit a generally plate-like and fine crystal morphology among these samples. It is noted that the FF sample possesses the most uniform size distribution and the average particle size is as small as 0.5 μm (Fig. 1(a)). Comparatively, the average particle sizes of BF and PF samples are 1.5 and 6.0 μm, respectively (Figs. 1(b) and (c)).

With the least agglomeration, the higher specific surface area (SSA) in FF sample is further confirmed by the BET analysis of nitrogen adsorption−desorption isotherms (Fig. 2). The SSAs of FF, BF and PF samples are calculated to be 23.5, 8.8 and 7.2 m^2/g, respectively. Correspondingly, the pore volume of FF sample is calculated to be 0.12 cm^3/g, which is much higher than

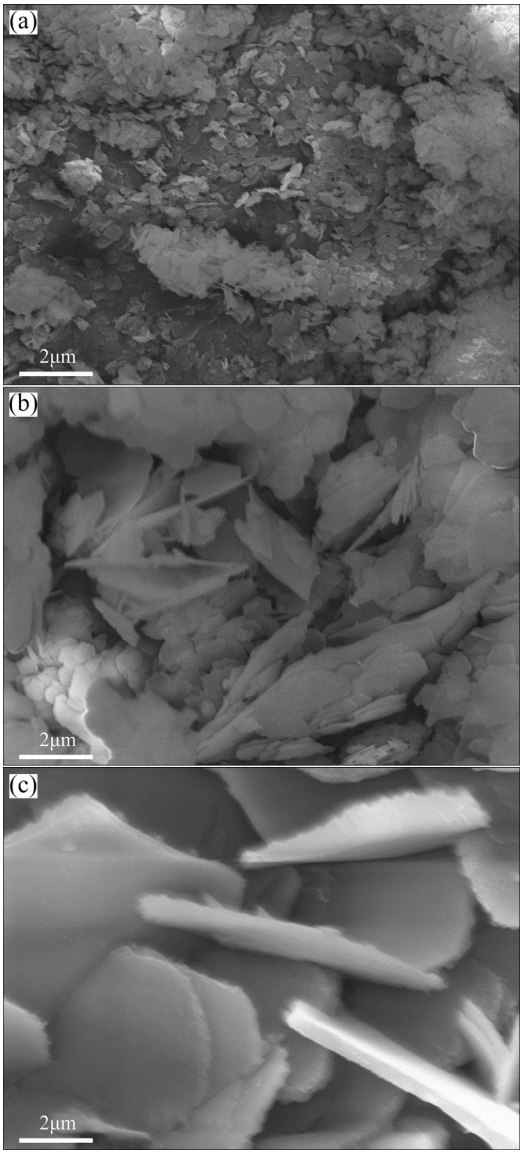

Fig. 1 FESEM images of Ca−Al−Cl−LDHs synthesized in different feeding ways: (a) Forward feeding; (b) Backward feeding; (c) Parallel feeding

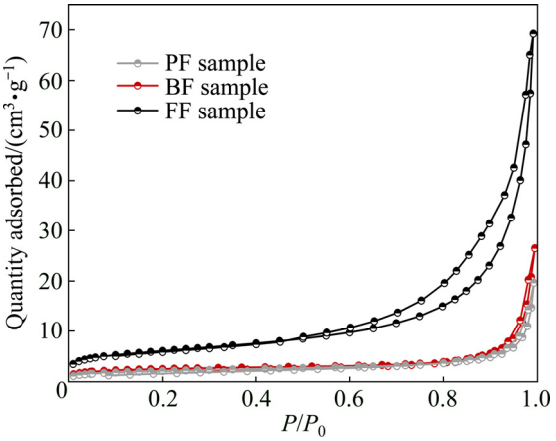

Fig. 2 Nitrogen adsorption−desorption isotherms of Ca−Al−Cl−LDHs synthesized with three feeding ways

that of BF sample by 0.035 cm^3/g and PF sample by 0.026 cm^3/g. Moreover, all adsorption−desorption isotherms correspond to the IUPAC type-IV shape with hysteresis loops from a capillary condensation process at P/P_0>0.5. The more significant adsorption in FF sample at medium relative pressure (0.9>P/P_0>0.5) indicates the abundant mesopores, while the slight rise at higher relative pressure (1.0>P/P_0>0.9) further implies the presence of macropores. All these results suggest a highly porous and accessible structure in FF sample with more active sites for Se(VI) adsorption [22,23]. As such, it can be deduced that the FF sample has higher potential for adsorption experiment.

The XRD spectra further prove a typical layered double hydroxide structure. As shown in Fig. 3, sharp peaks in all samples are centered at 11.38°, 22.88°, 23.63° and 31.33°, corresponding to the (002), (004), (112) and (020) lattice planes in the hexagonal crystal system, respectively [3]. This result matches with the standard card profile of the monoclinic LDHs structure (PDF 31−0245) as $Ca_2Al(OH)_6(H_2O)_2Cl$. The indexing of XRD patterns shows the close d values of three samples. It is further calculated that all three samples exhibit the hexagonal crystals of monoclinic group ($P21/c$) with a=1.018−1.036 nm, b=0.574−0.576 nm, c=1.723−1.730 nm and β=114.65°−114.90°. Moreover, the $d_{(002)}$ spacing of FF, BF and PF samples ranges from 0.784 to 0.788 nm. According to the Scherrer formula, the grain sizes are thus calculated to be 37.3−48.0 nm [24].

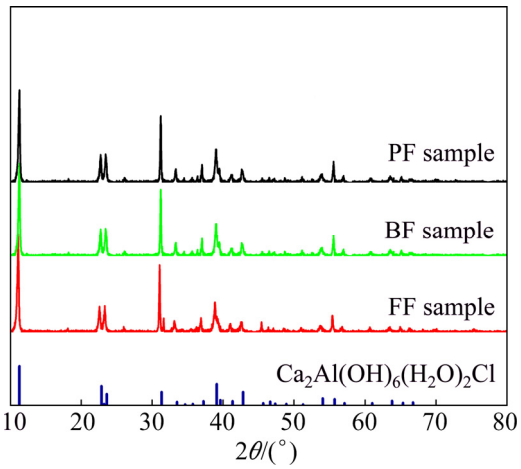

Fig. 3 XRD patterns of Ca−Al−Cl−LDHs synthesized with three feeding ways

The FT-IR spectra of synthesized Ca−Al−Cl−LDHs recorded in Fig. 4(a) show the peak distributions of three samples are similar. Notably, the features at 3640 and 3490 cm^{-1} can be ascribed to the stretching vibration of hydrogen-bonded —OH in the structural water from the hydroxide layers and interlayer water [16,22]. The peak

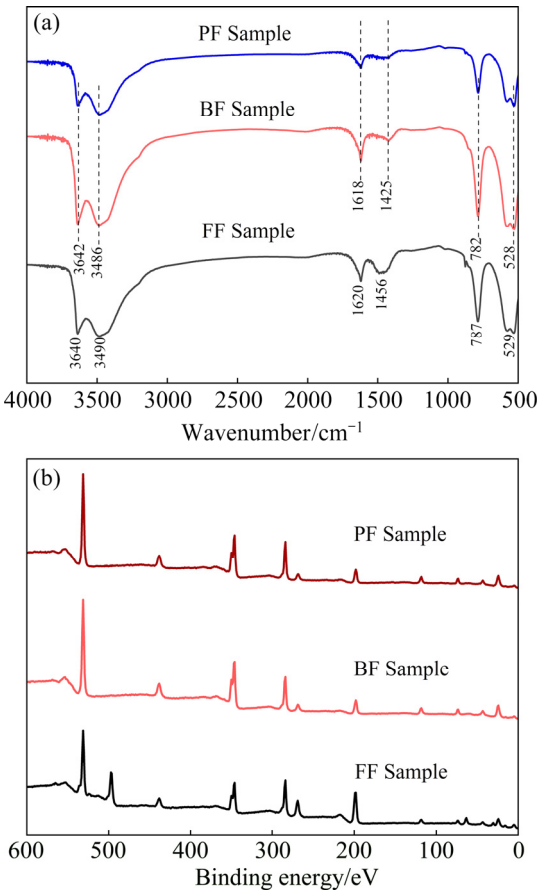

Fig. 4 FT-IR spectra (a) and XPS survey spectra (b) of Ca−Al−Cl−LDHs synthesized with three feeding ways

at 1620 cm^{-1} is due to the H—O—H bending vibration of —OH in the interlayer water molecule [16,22]. The weak peak at 1425−1456 cm^{-1} is further identified as the stretching vibration of the interlayer carbonate anions, which implies the incorporation of CO_2 into the alkaline solution during the synthesis [16,17]. In the low-wavenumber region (<900 cm^{-1}), the peaks at 528−529 cm^{-1} and 782−787 cm^{-1} are associated with lattice vibration modes of Al—O—H stretching [3,15]. These results generally agree with the characteristic peaks of typical Friedel's salts. The chemical environment of Ca−Al−Cl−LDHs was further investigated by the XPS analysis. From the survey spectra, five characteristic peaks at 530, 343, 285, 198, 62 eV are observed, corresponding to O 1s, Ca 2p, C 1s, Cl 2p, Al 2p signals (Fig. 4(b)). It is noted that higher content of Cl atoms in FF sample (9.4 at.%) than that in BF sample (6.8 at.%) and PF sample (6.1 at.%) is obtained. Since the anion exchange plays an important role in the adsorption process of Se(VI), the presence of more exchangeable Cl anions in Ca−Al−Cl−LDHs is favorable to the deselenization process. The high-resolution O1s spectra of Ca−Al−Cl−LDHs are further deconvoluted into three peaks at 532.6, 531.1, and 530.7 eV, which represent the

different oxygen forms in C═O—, —OH, and M—O, respectively [25]. The higher content of —OH in FF sample (67%) than that in BF sample (58%) and PF sample (62%) is consistent with the result of FTIR analysis, which also contributes to more active sites.

3.2 Preliminary experiment to evaluate adsorption capability

The preliminary adsorption experiment was conducted to evaluate the adsorption capability of three Ca−Al−Cl−LDH samples (Table 1). Accordingly, 20 g LDHs were added to 500 mL alkaline selenium solution at 50 °C for 120 min. Table 1 shows that the FF sample reaches the adsorption equilibrium at 30 min and the final adsorption efficiency at 120 min is calculated to be 81.4%, which is superior than that in BF sample by 75.1% and PF sample by 71.9%. Consistent with the morphological and structural analysis, FF sample exhibits the best Se(VI) adsorption capacity due to its smaller average particle size, larger specific surface area, enlarged interlayer distance and more exchangeable sites [26]. Therefore, FF sample is selected for further study on the factor experiments, adsorption kinetics and adsorption isotherms.

Table 1 Se (VI) adsorption on LDHs synthesized with different feeding methods

Feeding mode	C_0/ (g·L^{-1})	C_{30}/ (g·L^{-1})	C_{120}/ (g·L^{-1})	Adsorption efficiency/%
FF	2.05	0.415	0.390	81.4
BF	2.04	1.01	0.518	75.1
PF	2.05	1.77	0.601	71.9

3.3 Se(VI) adsorption at different temperatures

To evaluate the impacts of adsorption temperatures, five temperatures ranging from 30 to 90 °C were set, while the adsorbent material dosage, the NaOH concentration and initial Se(VI) concentration were performed as 40, 40 and 2 g/L, respectively [9]. Figure 5 plots the Se(VI) concentration as a function of deselenization time and deselenization temperature in FF sample. It is found that at lower temperatures (30 and 50 °C), the Se(VI) concentrations decrease drastically in the first 30 min and the equilibrium is reached with a adsorption efficiency of ~90%, indicating the outstanding deselenization capability. However, at above 70 °C, the deselenization efficiency is receded with the increasing temperatures that the adsorption efficiency at 90 °C drops to 25% at 15 min. More impressively, a significant desorption effect is observed with the prolonged time. Especially, at 70 °C, the desorption process occurs at 120 min and the final Se(VI) concentration is 1.6 g/L. Similarly, the desorptions at 80 and 90 °C happen at 15 and 20 min, respectively, with almost no Se(VI) removed at 360 min.

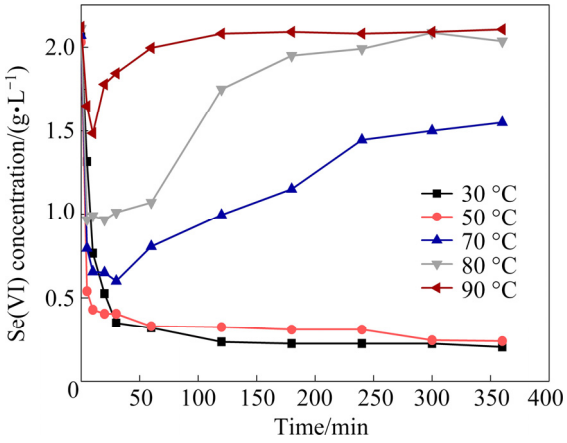

Fig. 5 Effects of adsorption temperatures on Se(VI) adsorption in Ca−Al−Cl−LDHs

To explore the desorption mechanism at high temperatures, combined with FESEM, BET, XRD, FT-IR and XPS analysis, adsorbent materials were employed. As shown in Fig. 6(b), the XRD patterns of FF-30°C and FF-50 °C samples are consistent with the standard card profile of monoclinic LDHs structure (PDF 31−0245), suggesting no structural changes in the low temperature adsorption. Accordingly, the FESEM images of FF-30 °C and FF-50 °C samples exhibit the flat and fine crystal morphology (Fig. 6(a)) [5]. However, with the elevated temperatures, impurity peaks as $Ca(OH)_2$ and $Ca_3Al_2(OH)_{12}$ become significant in the XRD spectra of FF-70 °C, FF-80 °C and FF-90 °C samples, which could be ascribed to decomposition of $Ca_2Al(OH)_6(H_2O)_2Cl$ at high temperatures (Fig. 6(b)) [27]. By comprehensively comparing these spectra, the diffraction peaks become sharper with increasing temperatures, indicating higher crystallinity. As shown in the FESEM images, the sizes of FF samples become larger in FF-70 °C, FF-80 °C and FF-90 °C samples and some block-shape crystals are also observed (Fig. 6(a)). This result is attributed to the decomposition and recrystallization process of Ca−Al−Cl−LDHs at above 70 °C.

The nitrogen adsorption−desorption isotherms further change from the IUPAC type-IV shape in the original FF sample to the IUPAC type-II shape in the processed FF samples (Fig. 7). The SSAs also decrease from 23.5 m^2/g in the original FF sample to 10.7, 7.4, 3.8, 3.2 and 2.6 m^2/g in FF-30 °C, FF-50 °C, FF-70 °C, FF-80 °C and FF-90 °C samples, respectively. The decreasing SSAs in FF-30 °C, FF-50 °C could be attributed to the deposited selenium salts on the nonuniform surface of adsorbents through the adsorption, complexation and precipitation effects [18,23], whereas

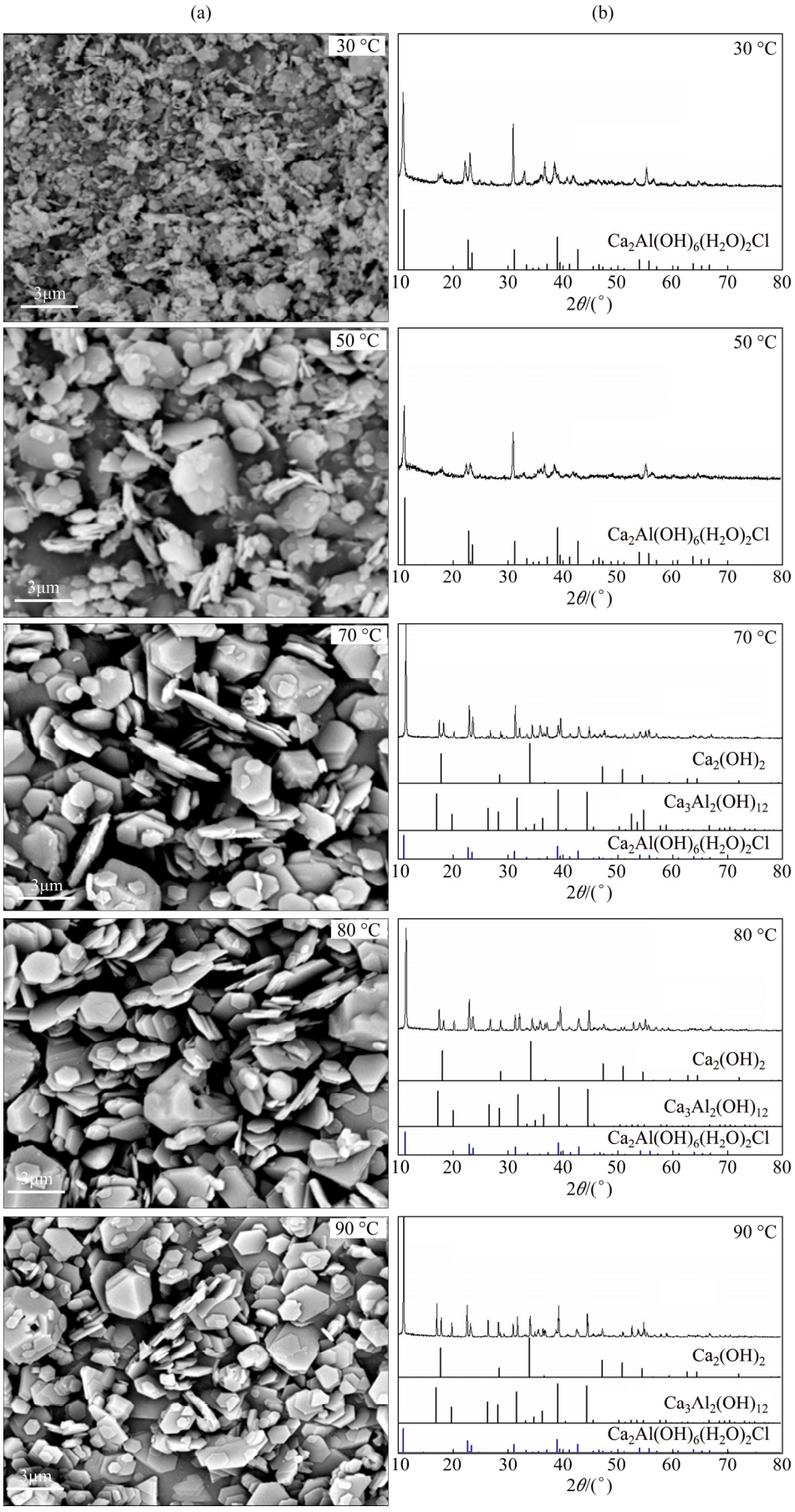

Fig. 6 FESEM images (a) and XRD patterns (b) of FF samples collected after adsorption experiments at different temperatures

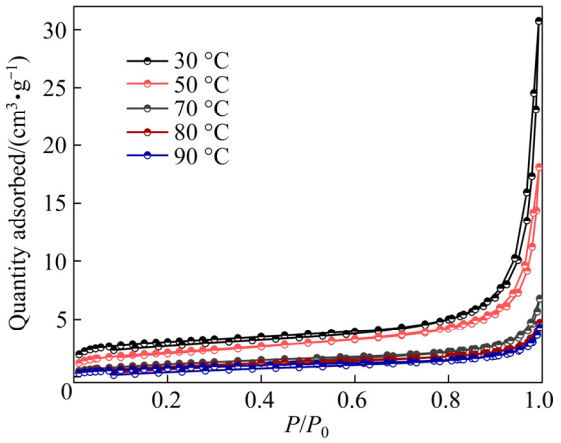

Fig. 7 Nitrogen adsorption−desorption isotherms of FF samples collected after adsorption experiments at different temperatures

the decreasing SSAs in FF-70 °C, FF-80 °C and FF-90 °C further concern the decomposition/reconstruction effect of Ca−AL−Cl−LDHs at high adsorption temperatures.

The FT-IR spectra of processed samples further exhibit a general shift of the hydrogen-bonded —OH from 3480 cm^{-1} in FF-30 °C and FF-50 °C samples to 3510 cm^{-1} in FF-70 °C, FF-80 °C and FF-90 °C samples (Fig. 8(a)) [5]. Since the selenate and hydroxides are both recognized as the hard alkali to potentially react with the hard acid as the metal ions, this shift implies that the hydroxyls in structural water from the hydroxide layers and interlayer water have reduced the active sites for Se(VI) adsorption [27]. This competing reaction becomes more severe at higher temperatures. The peaks in the low-wavenumber region become weaker. Especially, the peak intensities at 875, 536 and 785 cm^{-1} dramatically decrease with increasing temperatures. These results suggest that the reduction of active sites at higher temperatures is also ascribed to the decomposition of Ca−Al−Cl−LDHs. It is noted that a new peak at 2930 cm^{-1} appears in FF-70 °C, FF-80 °C and FF-90 °C samples, which could be recognized as the hydrogen-bonded hydroxyls to the carbonate anions [16,22]. This peak not only confirms the partial decomposition of LDHs, but also implies more severe adsorption of CO_2 at higher temperatures.

The XPS survey spectra further exhibit the disappearance of Se 3d peaks in FF-80 °C and FF-90 °C samples, which is consistent with the results in the adsorption equilibriums (Fig. 8(b)). In the high-resolution O 1s spectra, the content of — OH significantly decreases with the increasing temperature, also indicating the reduced active sites (Fig. 8(c)). Altogether, the higher deselenization rate at 50 °C with the close deselenization efficiency at 30 and 50 °C

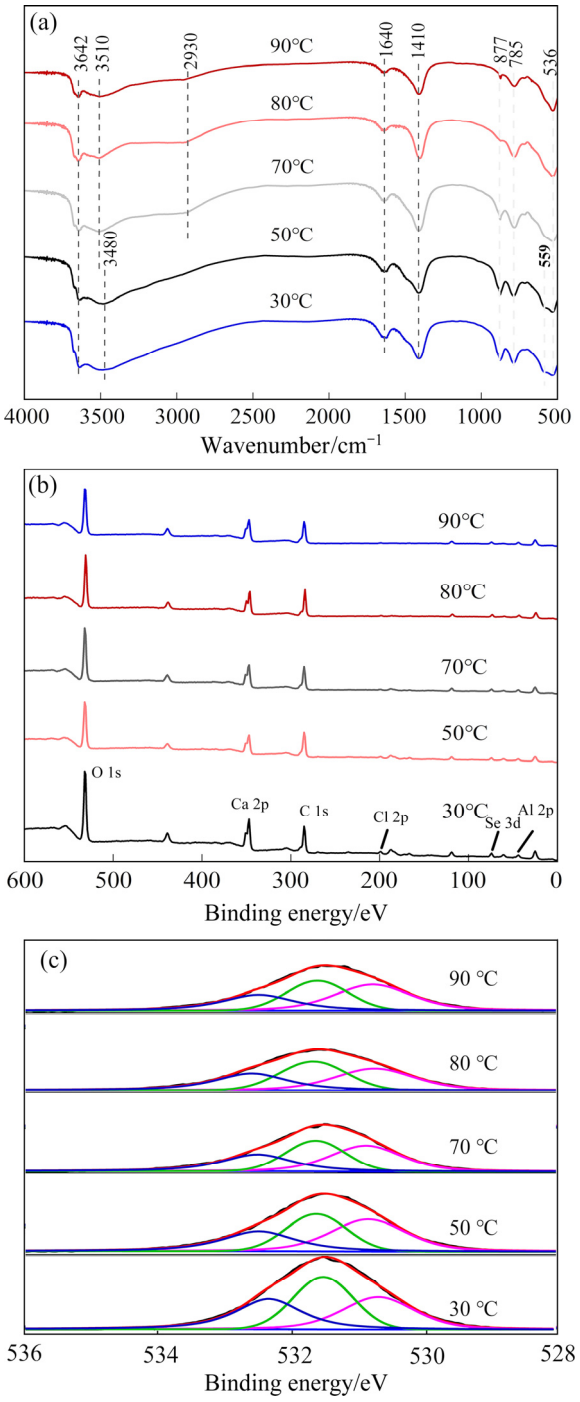

Fig. 8 FT-IR spectra (a), XPS survey spectra (b), high-resolution O 1s spectra (c) of FF samples collected after adsorption experiments at different temperatures

implies an endothermic process. Considering the thermolability of LDHs, we select 50 °C as the optimum temperature for further investigation.

3.4 Se(VI) adsorption at different LDH dosages

The impacts of adsorbent material dosages on Se(VI) adsorption are shown in Fig. 9, where the adsorption temperature, NaOH concentration and initial

Se(VI) concentration are set as 50 °C, 40 g/L and 2 g/L, respectively [28]. The deselenization efficiency increases with the increasing adsorbent dosage and the adsorption equilibriums are reached at 60 min. Especially, when the dosage is performed as 10 g/L, the deselenization efficiency is only 40.5%. After increasing the adsorbent dosage to 20 g/L, the deselenization efficiency sharply increases to 81.2%. Further increase in the adsorbent supply to 30 and 40 g/L reaches a level-off and the deselenization efficiencies only increase to 85% and 90%, respectively.

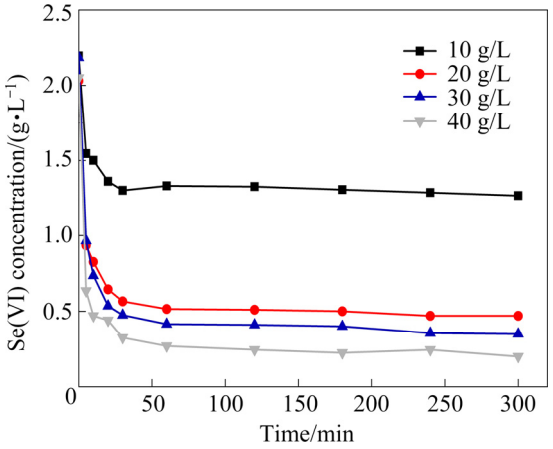

Fig. 9 Effects of adsorbent dosage on Se(VI) adsorption in Ca−Al−Cl−LDHs

The XRD spectra exhibit no impurity peaks but a great consistency with the standard card profile of the monoclinic LDHs structure (PDF 31−0245, Fig. 10). Therefore, the adsorbent material dosage has limited impact on the structural alternation of LDHs. This result also confirms the outstanding recycling capability of Ca−Al−Cl−LDHs processed with different adsorbent dosages [29]. By comprehensively considering the deselenization efficiency and the economic cost, we select the optimum adsorbent material dosage as 30 g/L.

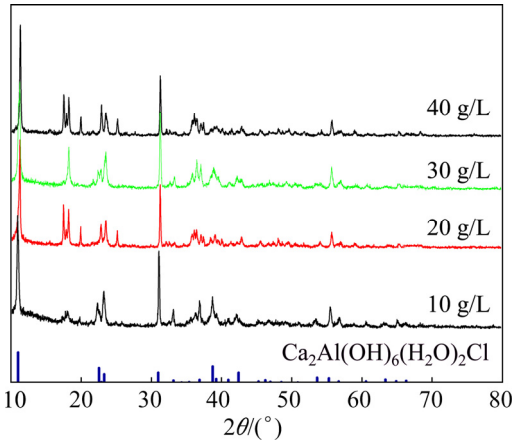

Fig. 10 XRD spectra of Ca−Al−Cl−LDHs collected after adsorption experiment with different adsorbent dosages

3.5 Se(VI) adsorption at different NaOH concentrations

The NaOH concentration plays an important role in the adsorption mechanisms. It is noted that the adsorption process of Se(VI) onto Ca−Al−Cl−LDHs includes the surface adsorption, the interlayer anion exchange and the intercalation by reconstruction of the structure [27]. Therefore, NaOH concentration can not only affect the oxyanion migration to the surface of adsorbent, but also trigger the competition between Se(VI) ion and hydroxide ion for anion exchange within the hydrocalumite [29,30]. In the present study, NaOH concentrations are set as 40, 60, 80 and 100 g/L with the adsorption temperature, adsorbent material dosage and initial Se(VI) concentration performed as 50 °C, 30 g/L and 2 g/L, respectively. As shown in Fig. 11, the deselenization rate and efficiency increase with the decreasing NaOH concentration. When the NaOH concentrations reach 100 and 80 g/L, the equilibriums are achieved at 60 min, while the deselenization efficiency in the former is only 30% and only increases to 60% in the latter. By contrast, when the NaOH concentration drops to 60 g/L, impressive improvement of deselenization rate and efficiency is observed as the equilibrium is achieved at 20 min with a high deselenization efficiency of 85%. Further decrease in NaOH concentration to 40 g/L leads to no obvious improvement.

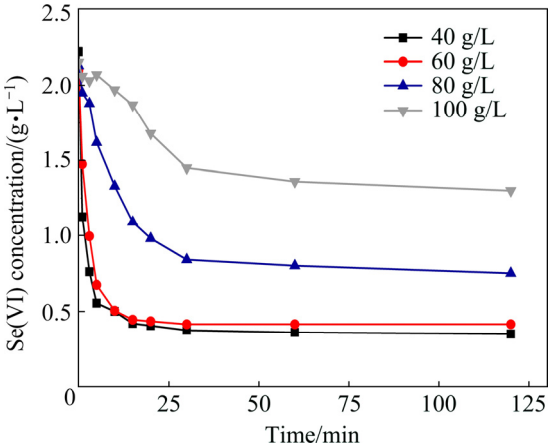

Fig. 11 Effects of NaOH concentration on Se(VI) adsorption in Ca−Al−Cl−LDHs

As shown in the FESEM images (Fig. 12), the Ca−Al−Cl−LDHs remain the plate-like morphology with the uniform size distribution. However, more significant particle aggregation and increasing average particle sizes are observed when the NaOH concentrations increase to 80 and 100 g/L. Given the significant impact of NaOH concentration on the surface charge of LDHs, zeta potentials were tested in four solutions of different NaOH concentrations. The results show that the zeta

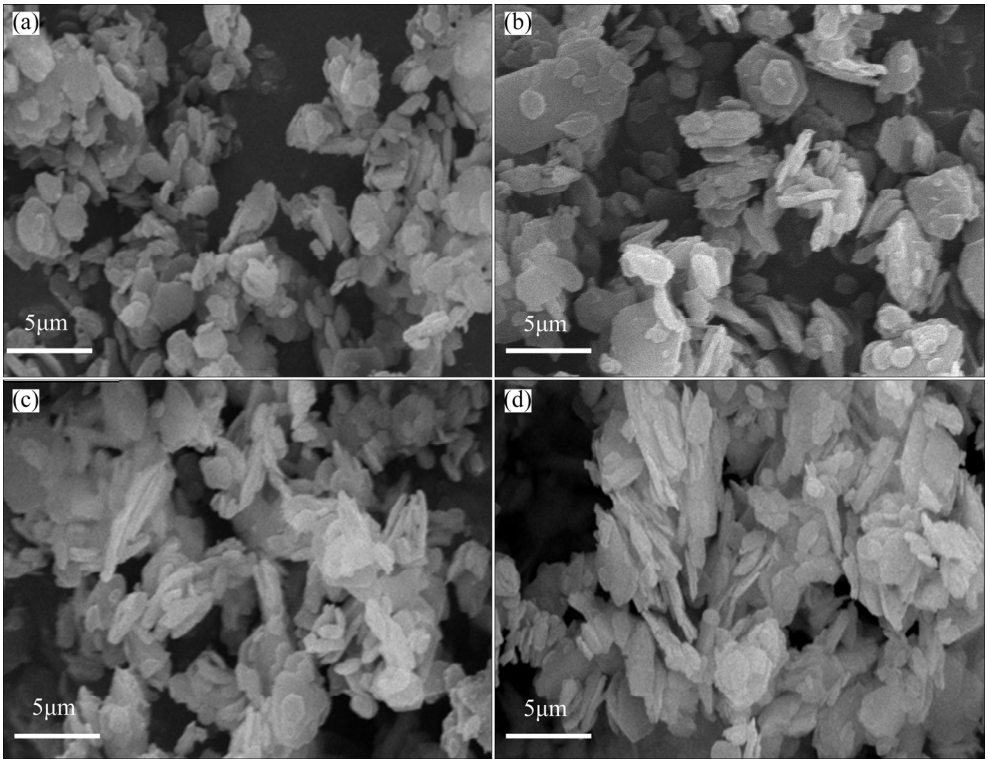

Fig. 12 FESEM images of Ca−Al−Cl−LDHs collected after adsorption experiment at different NaOH concentrations: (a) 40 g/L; (b) 60 g/L; (c) 80 g/L; (d) 100 g/L

potentials range from (−9.65±1.16) to (−14.93±1.23) mV when the NaOH concentration drops from 100 to 40 g/L. In the highly caustic solution (1.0−2.5 mol/L NaOH), deprotonation effect will occur on the surface of adsorbent material as suggested by the equation of surface —OH+OH^- → surface —O^-+H_2O [31]. A less stable system with more significant particle aggregation is thus found with the high NaOH concentrations up to 80 and 100 g/L, resulting in the decrease of available binding sites for Se(VI).

The XRD spectra further display no structural changes from the standard monoclinic LDHs structure (PDF 31−0245) as $Ca_2Al(OH)_6(H_2O)_2Cl$ (Fig. 13(a)). The FT-IR and XPS analyses were also employed. In the FTIR spectra, the peaks assigned to the hydrogen-bonded hydroxyls significantly move from 3480 cm^{-1} in the relatively low NaOH concentrations of 40 and 60 g/L to 3520 cm^{-1} in the high NaOH concentrations of 80 and 100 g/L [1,16−17] (Fig. 13(b)). Considering the reduced active sites at higher temperatures, these results combinedly confirm the endothermic process of a competition reaction between Se(VI) ion and hydroxide ion for anion exchange within the hydrocalumite [18]. The decreased active sites for Se(VI) thus account for the reduction of deselenization efficiency. It is also noted that an inconspicuous peak at 2930 cm^{-1} is observed, which could be ascribed to the hydrogen-bonded hydroxyls to the carbonate anion. This result is caused by the more severe dissolution of CO_2 in the caustic solutions. The high-resolution O1s XPS spectra further demonstrate that the deconvoluted peaks at 530.7 eV (M—O form) are significantly enhanced in processed Ca−Al−Cl−LDHs, indicating the deposited selenium-containing hydroxide precipitates on the surface (Fig. 13(c)). The relative contents of —OH form further increase from 58% in 100 g/L NaOH to 67% in 40 g/L NaOH, suggesting that more active sites have been occupied in the highly caustic solutions and the adsorption of Se(VI) is thus hindered. Moreover, high NaOH concentration could be unfavorable to the adsorption of Se(VI) that the increased liquid viscosity could limit oxyanions migration and lead to poor diffusion rate [32]. Therefore, to minimize the unfavorable impact of high NaOH concentration and to meet the situation in practical wastewater, we select 60 g/L NaOH as the optimum concentration. In summary, the optimum adsorption condition is determined that the adsorption temperature is 50 °C, the adsorbent dosage is 30 g/L, and the NaOH concentration is 60 g/L.

3.6 Adsorption kinetics of Se(VI) on Ca−Al−Cl−LDHs

The adsorption kinetics of Se(VI) on the synthesized LDHs was investigated and the adsorption process with respect to the reaction time was also

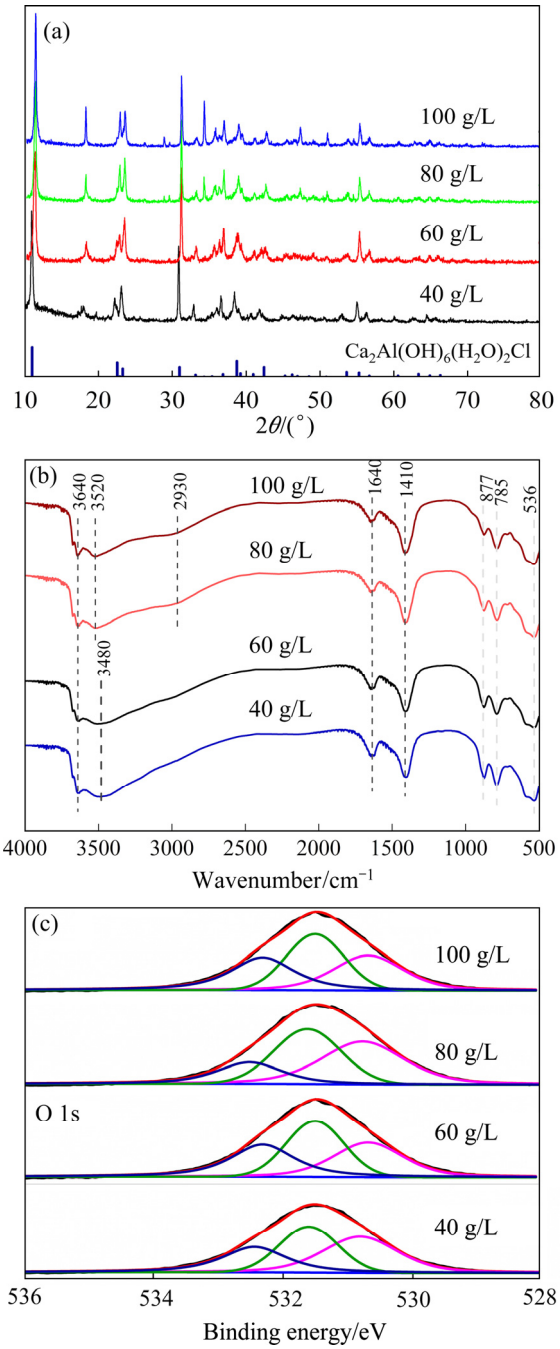

Fig. 13 XRD spectra (a), FTIR spectra (b), high resolution O 1s XPS spectra (c) of Ca−Al−Cl−LDHs collected after adsorption experiment at different NaOH concentrations

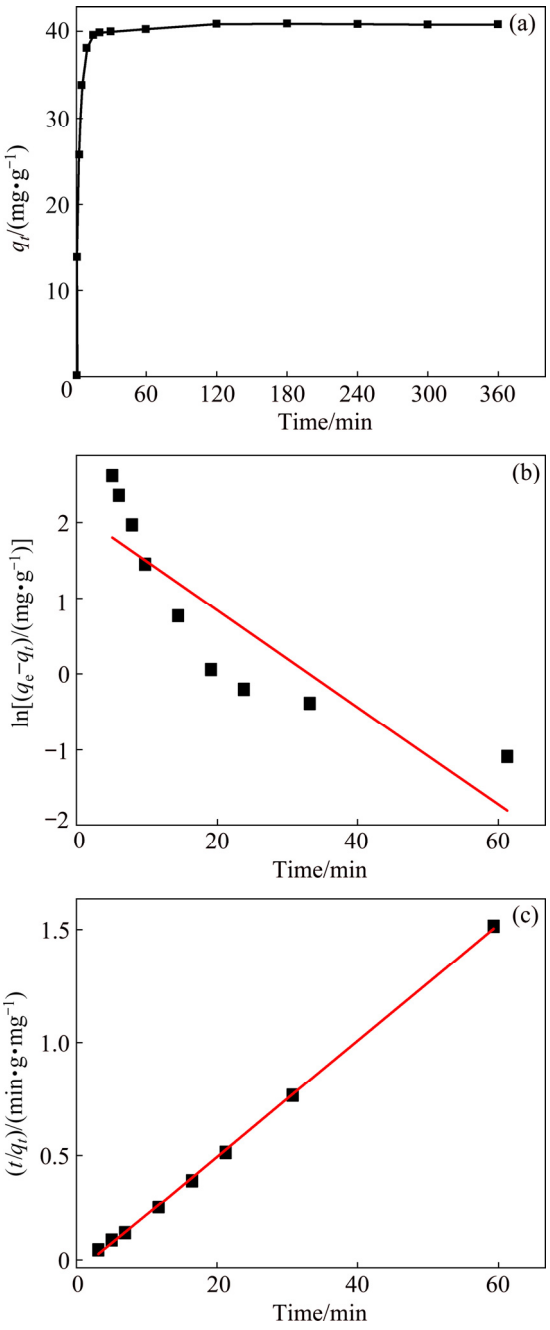

Fig. 14 Effects of adsorption time on Se(VI) adsorption in Ca−Al−Cl−LDHs (a), and adsorption kinetics fitting of Se(VI) in Ca−Al−Cl−LDHs by pseudo-first-order (b) and pseudo-second-order (c) models

fitted [33]. The kinetics curve shows a rapid adsorption in the first 15 min, after which the equilibrium is immediately reached (Fig. 14(a)). The initial rapid adsorption of Se(VI) could be attributed to the abundant available sites on the surface. Controlled by the reverse adsorption−desorption process and ion exchange rate, the reaction reaches the equilibrium. According to the pseudo-first-order and pseudo-second-order models, $\ln(q_e-q_t)$ and t/q_t are selected as the dependent variables, respectively, where q_e (mg/g) and q_t (mg/g) correspond to the adsorption amount of the adsorbate at equilibrium and at time t [20]. The fitted curves of nonlinear regression show that the equilibrium data are described better by the pseudo-second-order models, which is elucidated by the higher correlation coefficient (R^2) of 0.999 than that in the pseudo-first-order model of 0.727 (Figs. 14(b) and (c), Table 2). This indicates that the adsorption process is a second-order adsorption kinetics system and controlled by the chemical adsorption [34].

Table 2 Adsorption kinetic parameters for Se(VI) adsorption onto Ca−Al−Cl−LDHs

$q_{e,exp}$/(mg·g^{-1})	Pseudo-first-order equation			Pseudo-second-order equation		
	k_1/min^{-1}	$q_{e,cal}$/(mg·g^{-1})	R^2	k_2/(g·mg^{-1}·min^{-1})	$q_{e,cal}$/(mg·g^{-1})	R^2
40.4	0.0935	11.2	0.727	0.0175	41.4	0.999

3.7 Adsorption isotherms of Se(VI) on Ca−Al−Cl−LDHs

To evaluate the adsorption characteristics of the synthesized LDHs, two isotherm models including Langmuir and Freundlich models were employed to analyze the adsorption data. The fitted isotherm parameters exhibit a better correlation coefficient of 0.952 in the Langmuir model, which assumes a monolayer adsorption onto homogeneous surface with a finite number of identical sites and no lateral interaction as well as steric hindrance between the adsorbate molecules (Fig. 15) [21,35,36]. By contrast, the correlation coefficient in the Freundlich model is only 0.842. Therefore, we confirm that the adsorption of Se(VI) onto Ca−Al−Cl−LDHs is mainly the monolayer adsorption. Moreover, as calculated from the isotherms obtained at Se(VI) equilibrium concentration, the maximum adsorption capacity (q_m) on the synthesized Ca−Al−Cl−LDHs at 50 °C reaches 188.6 mg/g (Table 3). It is noted that in most reports, calcined forms of LDHs exhibit higher adsorption capability [28], whereas for the uncalcined forms of LDHs in present study, the as-obtained Ca−Al−Cl−LDHs possess an impressive adsorption capacity with a favorable process of low temperature, acceptable adsorbent dosages and high alkali concentration. These results thus suggest that the synthesized Ca−Al−Cl−LDHs are promising for industrial application.

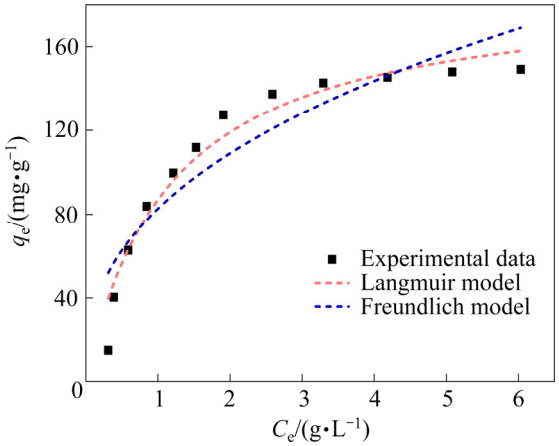

Fig. 15 Adsorption isotherms of Se(VI) onto Ca−Al−Cl−LDHs

Table 3 Langmuir and Freundlich adsorption isotherm parameters of Se(VI) onto Ca−Al−Cl−LDHs

Langmuir model			Freundlich model		
q_m/(mg·g^{-1})	K_L/(L·mg^{-1})	R^2	K_F	n	R^2
188.6	0.86	0.952	82.73	0.40	0.842

4 Conclusions

(1) The synthesized Ca−Al−Cl−LDHs exhibit a plate-like morphology and hexagonal crystal structure with the typical mineral phases and functional groups.

(2) Ca−Al−Cl−LDHs synthesized with the forward feeding method possess better adsorption capacity of Se(VI).

(3) The optimum adsorption conditions are determined that the adsorption temperature is 50 °C, the adsorbent dosage is 30 g/L, and the NaOH concentration is 60 g/L.

(4) The adsorption kinetics and isotherm parameters can be well described by the pseudo-second-order and the Langmuir isotherm models, respectively. The maximum adsorption amount of Se(VI) onto Ca−Al−Cl LDHs at 50 °C reaches 188.6 mg/g.

References

[1] LIU Wei-feng, YANG Tian-zu, ZHANG Du-chao, CHEN Lin, LIU You-nian. Pretreatment of copper anode slime with alkaline pressure oxidative leaching [J]. International Journal of Mineral Processing, 2014. 128: 48−54.

[2] LI Dong, GUO Xue-yi, XU Zhi-peng, TIAN Qing-hua, FENG Qi-ming. Leaching behavior of metals from copper anode slime using an alkali fusion-leaching process [J]. Hydrometallurgy, 2015, 157: 9−12.

[3] LI Dong, GUO Xue-yi, TIAN Qing-hua, XU Zhi-peng, XU Run-ze, ZHANG Lei. Synthesis and application of Friedel's salt in arsenic removal from caustic solution [J]. Chemical Engineering Journal, 2017, 323: 304−311.

[4] WANG Yun-ting, XUE Yu-dong, SU Jun-ling, ZHENG Shi-li, LEI Hong, CAI Wei-quan, JIN Wei. Efficient electrochemical recovery of dilute selenium by cyclone electrowinning [J]. Hydrometallurgy, 2018, 179: 232−237.

[5] LI Dong, GUO Xue-yi, TIAN Qing-hua, XU Run-ze, XU Zhi-peng, ZHANG Jing. Dearsenization of caustic solution by synthetic hydrocalumite [J]. Hydrometallurgy, 2016, 161: 1−6.

[6] DESSI P, JAIN R, SINGH S, SEDER-COLOMINA M, HULLEBUSCH E D V, RENE E R, AHAMMAD S Z, CARUCCI A, LENS P N L. Effect of temperature on selenium removal from wastewater by UASB reactors [J]. Water Research, 2016, 94: 146−154.

[7] LU Dian-kun, CHANG Yong-feng, YANG Hong-ying, XIE Feng. Sequential removal of selenium and tellurium from copper anode slime with high nickel content [J]. Transactions of Nonferrous Metals Society of China, 2015, 25(4): 1307−1314.

[8] ZHAO Gui-xia, HUANG Xiu-bing, TANG Zhen-wu, HUANG Qi-fei, NIU Feng-lei, WANG Xiang-ke. Polymer-based

nanocomposites for heavy metal ions removal from aqueous solution: a review [J]. Polymer Chemistry, 2018, 9(26): 3562−3582.

[9] BLEIMAN N, MISHAEL Y G. Selenium removal from drinking water by adsorption to chitosan-clay composites and oxides: Batch and columns tests [J]. Journal of Hazardous Materials, 2010, 183(1−3): 590−595.

[10] LI Jie, WANG Xiang-xue, ZHAO Gui-xia, CHEN Chang-lun, CHAI Zhi-fang, ALSAEDI A, HAYAT T, WANG Xiang-ke. Metal-organic framework-based materials: Superior adsorbents for the capture of toxic and radioactive metal ions [J]. Chemical Society reviews, 2018, 47(7): 2322−2356.

[11] WU Yi-han, PANG Hong-wei, LIU Yue, WANG Xiang-xue, YU Shu-jun, FU Dong, CHEN Jian-rong, WANG Xiang-ke. Environmental remediation of heavy metal ions by novel-nanomaterials: A review [J]. Environmental pollution 2019, 246: 608−620.

[12] GU Peng-cheng, ZHANG Sai, LI Xing, WANG Xiang-xue, WEN Tao, JEHAN R, ALSAEDI A, HAYAT T, WANG Xiang-ke. Recent advances in layered double hydroxide-based nanomaterials for the removal of radionuclides from aqueous solution [J]. Environmental pollution, 2018, 240: 493−505.

[13] ZHANG Fen, ZHANG Chang-lei, SONG Liang, ZENG Rong-chang, LIU Zhen-guo, CUI Hhong-zhi. Corrosion of in-situ grown MgAl-LDH coating on aluminum alloy [J]. Transactions of Nonferrous Metals Society of China, 2015**,** 25 (10): 3498−3504.

[14] ZHANG Li, DAI Chao-hua, ZHANG Xiu-xiu, LIU You-nian, YAN Jian-hui. Synthesis and highly efficient photocatalytic activity of mixed oxides derived from ZnNiAl layered double hydroxides [J]. Transactions of Nonferrous Metals Society of China, 2016, 26(9): 2380−2389.

[15] HONG Jun, ZHU Zhi-liang, LU Hong-tao, QIU Yan-ling. Synthesis and arsenic adsorption performances of ferric-based layered double hydroxide with α-alanine intercalation [J]. Chemical Engineering Journal, 2014, 252: 267−274.

[16] LI Yang, ZOYA S, PAUL K T L, MUHAMMAD S, THEODORE T T. Removal of trace levels of arsenic and selenium from aqueous solutions by calcined and uncalcined layered double hydroxides (LDH) [J]. Industrial & Engineering Chemistry Research, 2005, 44: 6804−6815.

[17] GUO Yan-wei, ZHU Zhi-liang, QIU Yan-ling, ZHAO Jian-fu. Adsorption of arsenate on Cu/Mg/Fe/La layered double hydroxide from aqueous solutions [J]. Journal of Hazardous Materials, 2012, 239−240: 279−88.

[18] HUANG Qi, LIU Kai-yu, HE Fang, ZHANG Shui-rong, XIE Qing-liang, CHEN Cheng. Fabrication of cobalt aluminum-layered double hydroxide nanosheets/carbon spheres composite as novel electrode material for supercapacitors [J]. Transactions of Nonferrous Metals Society of China, 2017, 27(8): 1804−1814.

[19] LONG Ya-ling, YU Jin-gang, JIAO Fei-peng, YANG Wei-jie. Preparation and characterization of MWCNTs/LDHs nanohybrids for removal of Congo red from aqueous solution [J]. Transactions of Nonferrous Metals Society of China, 2016, 26(10): 2701−2710.

[20] ZARE F, GHAEDI M, DANESHFAR A, AGARWAL S, TYAGI I, SALEH T A, GUTPA V K. Efficient removal of radioactive uranium from solvent phase using AgOH–MWCNTs nanoparticles: Kinetic and thermodynamic study [J]. Chemical Engineering Journal, 2015, 273: 296−306.

[21] DANMALIKI G I, SALEH T A. Effects of bimetallic Ce/Fe nanoparticles on the desulfurization of thiophenes using activated carbon [J]. Chemical Engineering Journal, 2017, 307: 914−927.

[22] LI Yang, MEGHA D, ZOYA S, MAYUR O, PAUL K T L, MUHAMMAD S, THEODORE T T. Adsorption of arsenic on layered double hydroxides: Effect of the particle size [J]. Industrial & Engineering Chemistry Research, 2006, 45: 4742−4751.

[23] HUANG Shu-yi, SONG Shuang, ZHANG Rui, WEN Tao, WANG Xiang-xue, YU Shu-jun, SONG Wen-cheng, HAYAT T, ALSAEDI A, WANG Xiang-ke. Construction of layered double hydroxides/hollow carbon microsphere composites and its applications for mutual removal of Pb(II) and humic acid from aqueous solutions [J]. ACS Sustainable Chemistry & Engineering, 2017, 5(12): 11268−11279.

[24] GRISHCHENKO R O, EMELINA A L, MAKAROV P Y. Thermodynamic properties and thermal behavior of Friedel's salt [J]. Thermochimica Acta, 2013, 570: 74−79.

[25] ZOU Yi-dong, LIU Yang, WANG Xiang-xue, SHENG Guo-dong, WANG Shu-hua, AI Yue-jie, JI Yong-fei, LIU Yun-hai, HAYAT T, WANG Xiang-ke. Glycerol-modified binary layered double hydroxide nanocomposites for uranium immobilization via extended X-ray absorption fine structure technique and density functional theory calculation [J]. ACS Sustainable Chemistry & Engineering, 2017, 5(4): 3583−3595.

[26] WANG Jian, WANG Peng-yi, WANG Hui-hui, DONG Jjun-fei, CHEN Wan-ying, WANG Xiang-xue, WANG Shu-hua, HAYAT T, ALSAEDI A, WANG Xiang-ke. Preparation of molybdenum disulfide coated Mg/Al layered double hydroxide composites for efficient removal of chromium(VI) [J]. ACS Sustainable Chemistry & Engineering, 2017, 5(8): 7165−7174.

[27] CAPORALE A G, PIGNA M, AZAM S M G G, SOMMELLA A, RAO M A, VIOLANTE A. Effect of competing ligands on the sorption/desorption of arsenite on/from Mg–Fe layered double hydroxides (Mg–Fe-LDH) [J]. Chemical Engineering Journal, 2013, 225: 704−709.

[28] VIOLANTE A, PUCCI M, COZZOLINO V, ZHU Jun, PIGNA M. Sorption/desorption of arsenate on/from Mg−Al layered double hydroxides: Influence of phosphate [J]. Journal of Colloid Interface Science, 2009, 333(1): 63−70.

[29] CHUBAR N, SZLACHTA M. Static and dynamic adsorptive removal of selenite and selenate by alkoxide-free sol–gel-generated Mg−Al−CO_3 layered double hydroxide: Effect of competing ions [J]. Chemical Engineering Journal, 2015, 279: 885−896.

[30] ZHANG Dan, ZHU Ming-yue, YU Jin-gang, MENG Hui-wen, JIAO Fei-peng. Effective removal of brilliant green from aqueous solution with magnetic Fe_3O_4@SDBS@LDHs composites [J]. Transactions of Nonferrous Metals Society of China, 2017, 27(12): 2673−2681.

[31] SONG Hai-lei, JIAO Fei-peng, JIANG Xin-yu, YU Jin-gang, CHEN Xiao-qing, DU Shao-long. Removal of vanadate anion by calcined Mg/Al−CO_3 layered double hydroxide in aqueous solution [J]. Transactions of Nonferrous Metals Society of China, 2013, 23(11): 3337−3345.

[32] MA Jiayu, LI Zhi-bao, ZHANG Yi, DEMOPOULOS G P. Desilication of sodium aluminate solution by Friedel's salt (FS: $3CaO{\cdot}Al_2O_3{\cdot}CaCl_2{\cdot}10H_2O$) [J]. Hydrometallurgy, 2009, 99(3−4): 225−230.

[33] ZOU Yi-dong, WANG Xiang-xue, WU Fen, YU Shu-jun, HU Ye-zi, SONG Wen-cheng, LIU Yun-hai, WANG Hong-qing, HAYAT T, WANG Xiang-ke. Controllable synthesis of Ca−Mg−Al layered double hydroxides and calcined layered double oxides for the efficient removal of U(VI) from wastewater solutions [J]. ACS Sustainable Chemistry & Engineering, 2016, 5 (1): 1173−1185.

[34] CHENG Xiang, HUANG Xin-rui, WANG Xing-zu, SUN De-zhi. Influence of calcination on the adsorptive removal of phosphate by Zn−Al layered double hydroxides from excess sludge liquor [J]. Journal of Hazardous Materials, 2010, 177(1−3): 516−523.

[35] ZOU Yi-dong, WANG Peng-yi, YAO Wen, WANG Xiang-xue, LIU Yun-hai, YANG Dong-xu, WANG Li-dong, HOU Jing, ALSAEDI A, HAYAT T, WANG Xiang-ke. Synergistic immobilization of UO^{22+} by novel graphitic carbon nitride @ layered double hydroxide nanocomposites from wastewater [J]. Chemical Engineering Journal, 2017, 330: 573−584.

[36] YU Shu-jun, LIU Yang, AI Yue-jie, WANG Xiang-xue, ZHANG Rui, CHEN Zhong-shan, CHEN Zhe, ZHAO Gui-xia, WANG Xiang-ke. Rational design of carbonaceous nanofiber/Ni−Al layered double hydroxide nanocomposites for high-efficiency removal of heavy metals from aqueous solutions [J]. Environmental Pollution, 2018, 242 (Part A): 1−11.

Ca−Al−Cl 型层状双金属氢氧化物用于强碱性溶液中六价硒的去除

徐少东，李 栋，郭学益，晏 文，高 杰

中南大学 冶金与环境学院，长沙 410083

摘 要：为提取铜阳极泥强碱性浸出液中的六价硒，通过三种共沉淀方法得到分子式为 $Ca_2Al(OH)_6Cl·2H_2O$ 的 Ca−Al−Cl 层状双氢氧化物(Ca−Al−Cl−LDHs)。综合 FESEM、XRD、FTIR、BET 和 XPS 分析发现，所得 Ca−Al−Cl 层状双氢氧化物具有片状形态、六方晶体结构以及典型矿物相和官能团。其中，正向进料方式得到的样品具有最佳的硒吸附能力。因素实验表明：低温、低氢氧化钠浓度和高吸附剂用量有利于六价硒的吸附。通过对吸附所得数据进行热力学及动力学拟合，发现吸附过程符合 Langmuir 吸附模型及准二级动力学模型。在 50 °C 时，Ca−Al−Cl−LDHs 对六价硒的最大吸附量达到 188.6 mg/g。

关键词：铜阳极泥；层状双金属氢氧化物；硒吸附；动力学；等温线

(Edited by Xiang-qun LI)